OpenAccess

Synthesis and spectroscopic characterisation of aurichalcite $(Zn,Cu^{2+})_5(CO_3)_2(OH)_6$; implications for Cu–ZnO catalyst precursors

**B. Jagannadha Reddy · Ray Leslie Frost ·
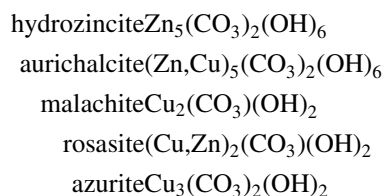Ashley Locke**

Abstract The Cu–ZnO catalyst precursors with variable Cu:Zn ratio, between Zn-rich and Cu-rich compositions have been investigated by a combination of electronic and vibrational spectroscopy. Synthesized catalyst precursors exhibit two d–d transition bands of Cu^{2+} ions in a distorted octahedral symmetry, at 7,600 and 12,900 cm^{-1} (1,315 and 775 nm). The effect of structural cation substitution (Zn^{2+} and Cu^{2+}) on band shifts is observed in the spectra of the synthetic catalyst precursors. The observation of two broad features at ∼7,600 and 12,900 cm^{-1} (1,315 and 775 nm) is a strong indication for Zn^{2+} substitution by Cu^{2+} ions. The result of multiple bands in the symmetric stretching and bending regions confirms the reduction of symmetry from D_{3h} to C_{2v}/C_s for $(CO_3)^{2-}$ ion in aurichalcite. The synthetic aurichalcite may be used as a standard for identification of spectral properties of naturally occurring anhydrous carbonate minerals.

Introduction

Aurichalcite $(Zn,Cu^{2+})_5(CO_3)_2(OH)_6$ is usually found as a secondary mineral in copper and zinc deposits. In nature the mineral appears as aggregates or tufts of light blue to green needles/blades [1–4]. The aurichalcite composition shows variation in the Cu:Zn ratio [5]. The aurichalcite mineral can be confused with other related minerals, such as rosasite because of their similar appearance. Rosasite minerals

B. J. Reddy · R. L. Frost (✉) · A. Locke
Inorganic Materials Research Program, School of Physical and Chemical Sciences, Queensland University of Technology, GPO Box 2434, Brisbane, QLD 4001, Australia
e-mail: r.frost@qut.edu.au

including glaukosphaerite, kolwezite and mcguinnessite show larger crystals. Other related hydroxy carbonate minerals are nullaginite and pokrovskite [6–9]. Aurichalcite is related to hydrozincite, $Zn_5(CO_3)_2(OH)_6$ and the minerals are formed under similar conditions when copper is present in solution [10, 11]. The crystal structure of aurichalcite was solved by Harding et al. [12]. The structure consists of double layers of closely packed oxygen layers parallel to (100). Within this double layer are the octahedral $M1$ and the tetragonally elongated $M2$ sites. On the opposite sides of this double layer are the tetrahedral $M3$ site and the trigonal bipyramidal site, $M4$. The layers are attached together on one side by hydrogen bonding between the hydroxyl groups and oxygen from a carbonate group, while on the other side there is metal–oxygen bonding. Aurichalcite is used in industry as a catalyst precursor for hydrogenation processes and a number of studies have consequently been focussed on the study of aurichalcite [13–15].

Spectroscopic investigations like NIR, IR and Raman spectroscopy show evidence of variable composition in natural minerals. For example, in aurichalcite, rosasite group of minerals, the effect of structural cation substitution (Ca^{2+}, Cu^{2+}, Fe^{2+}, Cd^{2+} and Zn^{2+}) has been observed [5–9, 16]. The naturally occurring hydroxyl-bearing zinc and copper carbonates are represented by the following five minerals according to the status of the species [2]:

hydrozincite $Zn_5(CO_3)_2(OH)_6$

aurichalcite $(Zn,Cu)_5(CO_3)_2(OH)_6$

malachite $Cu_2(CO_3)(OH)_2$

rosasite $(Cu,Zn)_2(CO_3)(OH)_2$

azurite $Cu_3(CO_3)_2(OH)_2$

The catalytic activity of copper–zinc oxides is known to depend on the catalyst precursor. The use of aurichalcite in

synthesising these catalyst precursors rests with the thermal decomposition of the aurichalcite to prepare mixed oxides which are mixed at the atomic level rather than the particle scale. This aspect is investigated in the present work through the study of the spectral properties of synthetic aurichalcite by varying the Cu:Zn ratio. The significance of the hydroxy carbonates precursor phases of Cu–ZnO catalysts was first highlighted by Herman et al. [17] and later extended to malachite and aurichalcite [18, 19]. Many have focussed on catalysts containing only copper and zinc oxide, the two components of greatest catalytic significance for hydrogenation [20–22]. Subsequently, many studies have researched Cu–ZnO/Al$_2$O$_3$ (CZA) catalysts [23–25] with Cu, Zn and Al in various selected proportions. The work described by Stone and Waller [26] on Cu–ZnO and alumina-supported Cu–ZnO as catalysts for the reverse shift reaction shows Cu:Zn ratios varying between Cu-rich and Zn-rich compositions.

Synthetic hydroxyl carbonates of Cu and Zn have potential use as catalysts or catalyst precursors. The Cu:Zn ratio specifies carbonate minerals, for example, malachite, rosasite or aurichalcite. Optimum ratio of Cu:Zn is an important component in biological and other systems. The behaviour of structural cations can be studied by means of electronic spectra and band shifts are expected for both Cu^{2+} ion and carbonate ions.

Divalent copper has a d^9 configuration. The Cu^{2+} ion has one free ion term, ^{2}D. In octahedral crystal field, this term splits into ground ^{2}E and excited ^{2}T states. The splitting of both ^{2}E and ^{2}T states is the effect of site distortion for Cu^{2+} ion that occupies Jahn–Teller sites in many copper complexes [27–31]. For Cu^{2+} the number of bands observable is four and three in rhombic and tetragonal fields, respectively [32]. The energies of the three bands in tetragonal field are related to ^{2}B$_1$ → ^{2}A$_1$, ^{2}B$_1$ → ^{2}B$_2$ and ^{2}B$_1$ → ^{2}E transitions. In this article, we discuss the spectral properties of synthetic aurichalcite, with variable Cu:Zn ratio, using UV–Vis and NIR spectroscopy, having in mind the thermal treatment of aurichalcite produces Cu–ZnO catalysts.

Experimental

Synthesis of aurichalcite

The mineral (Zn,Cu^{2+})$_5$(CO$_3$)$_2$(OH)$_6$ was synthesised with different ratios of Cu to Zn. Williams inferred from studies of natural aurichalcite minerals that the highest ratio of Cu to Zn in aurichalcite is 1:3 [11]. A common formula for natural aurichalcite is Cu$_{1.25}$Zn$_{3.75}$(CO$_3$)$_2$(OH)$_6$. In this work, aurichalcites were synthesised with ratios of 1:9, 1:4, 1:3, 2:3 and 1:1.

Synthesis of ideal products was modelled on the procedure by Fujita et al. [33]. A solution of metal ions (M^{2+}) was prepared by mixing appropriate concentrations of 1.5 M Cu(NO$_3$)$_2$ and Zn(NO$_3$)$_2$ corresponding to the metal concentrations desired in the products. Synthesis of the lower copper concentrations of aurichalcite (Cu < 50%) was carried out by adding dropwise 100 cm^3 of a 1.5 M M^{2+} solution via a peristaltic pump to 1,000 cm^3 of 0.2 M HCO$_3^-$ solution at 338 K. The relatively sensitive nature of aurichalcite to acidic (pH < 6) conditions precluded the use of the depleting methods mentioned in the literature [34] in order to obtain optimum yields of high phase purity aurichalcite. As such, a stream of saturated sodium bicarbonate was added at a quasi-constant rate in order to maintain a pH = 7.15; the samples were then aged for 30 min at 338 K under constant stirring. Aged samples were vacuum filtered and washed with hot, degassed and demineralised water. Samples were then dried overnight at 373 K.

The minerals were analysed by XRD for phase identification [35] and scanning electron microscopy (SEM) was employed for composition analysis. The chemical composition was obtained through EDX measurements.

X-ray diffraction

Powder X-ray diffraction analyses were performed on a Phillips X-ray diffractometer (radius: 173.0 mm). Incident X-ray radiation was produced from a long-fine focused C-Tech PW1050 Co X-ray tube, operating at 40 kV and 32 mA. The incident beam passed through a 1° divergence slit, a 15 mm fixed mask and a 1° fixed anti scatter slit. After interaction with the sample, the diffracted beam was detected by a proportional detector with a 0.2 mm receiving slit fitted to a graphite post-diffraction monochromer. The detector was set in scanning mode, with an active length of 2.022 mm. Samples were analysed utilising Bragg–Brentano 1° geometry over a range of 3–75° 2θ with a step size of 0.02° 2θ, with each step measured for 200 s.

UV–Vis spectroscopy

A Varian Cary 3 UV–Visible spectrophotometer, equipped with Diffuse Reflectance Accessory (DRA) was employed to record the electronic spectra of the samples in the region between 200 and 900 nm. This technique allows the study of the reflectance spectra of the samples in powder form. The DRA consists of a 73-mm diameter-integrating sphere, featuring an inbuilt high performance photomultiplier. Sample was mounted on coarse filter paper (#1), by

resuspending the sample and submerging the filter paper into the suspension. Initially, a base line was recorded using two pressed polytetrafluoroethylene (PTFE) reference disks. Next, the sample was mounted flat over the sample port and the reflectance spectrum of the sample, relative to the reference disks, was collected by the integrating sphere. By placing the sample flat any specular components of reflectance should be directed out of the DRA entrance port, as the angle of incidence is 0°. The diffuse reflectance measurements were converted into absorption (arbitrary units) using the Kubelka–Munk function $(f(R_\infty) = (1 - R_\infty)^2/2R_\infty)$. Data manipulation was performed using Microsoft Excel.

Near-infrared (NIR) and mid-infrared spectroscopy

NIR spectra were collected on a Nicolet Nexus FT-IR spectrometer with a Nicolet Near-IR Fibreport accessory (Madison, Wisconsin). A white light source was used, with a quartz beam splitter and TEC NIR InGaAs detector. Spectra were obtained from 13,000 to 4,000 cm^{-1} (0.77–2.50) by the co-addition of 64 scans at a spectral resolution of 8 cm^{-1}. A mirror velocity of 1.266 m s^{-1} was used. The spectra were transformed using the Kubelka–Munk algorithm to provide spectra for comparison with published absorption spectra.

Infrared spectra were obtained using a Nicolet Nexus 870 FT-IR spectrometer with a smart endurance single-bounce diamond ATR cell. Spectra over the 4,000–525 cm^{-1} range were obtained by the co-addition of 64 scans with a resolution of 4 cm^{-1} and a mirror velocity of 0.6329 cm s^{-1}. Spectra were co-added to improve the signal to noise ratio.

Spectral manipulation, such as baseline adjustment, smoothing and normalisation were performed using the Spectracalc software package GRAMS (Galactic Industries Corporation, NH, USA). Band component analysis was undertaken using the Jandel 'Peakfit' software package which enabled the type of fitting function to be selected and allows specific parameters to be fixed or varied accordingly. Band fitting was done using a Lorentz–Gauss cross-product function with the minimum number of component bands used for the fitting process. The Gauss–Lorentz ratio was maintained at values greater than 0.7 and fitting was undertaken until reproducible results were obtained with squared correlations of r^2 greater than 0.995.

Results and discussion

X-ray diffraction and EDX analysis

The X-ray diffraction patterns for the synthesised aurichalcite together with two reference patterns are shown in Fig. 1. The XRD patterns for Cu/Zn aurichalcite from 0.1/0.9, 0.25/0.75, 0.4/0.6 and 0.5/0.5 are shown. No minor impurities are observed. EDX analyses show that the average chemical composition corresponds to the formula given in Fig. 1.

UV–Vis spectroscopy

Reflectance spectra of carbonate minerals in the visible (Vis) and near-infrared (NIR) spectral regions show various features which are caused by multiphonon absorptions of the fundamental internal and lattice vibrational modes of the carbonate radical and OH units, and by electronic transitions in the unfilled d-shells of the transition metal cations [36, 37]. We have examined five samples of aurichalcite in which Cu:Zn ratios are in the range from 1:9 to 2:3. UV–Vis–NIR reflectance spectra are shown in Figs. 2 and 3 as plots of the Kubelka–Munk function (proportional to absorption) versus wavelength/wavenumber. The spectra in the UV–Vis region are shown in the Fig. 2a–e for the samples with Cu:Zn ratio of 1:9, 1:4, 1:3, 2:3 and 1:1. The Cu–ZnO catalysts with variable Cu:Zn (CZ) ratio between Zn-rich and Cu-rich compositions show an absorption edge at ∼400 nm (25,000 cm^{-1}) attributable to ZnO and a broad diagnostic band at 775 nm (12,900 cm^{-1}) related to the electronic transitions of Cu^{2+} ions in a distorted octahedral symmetry [5]. For the mixture of CZ with ratio of 2:3, both these absorptions are well resolved (Fig. 2d).

Copper atoms occupy Jahn–Teller distorted sites in many minerals including, aurichalcite, rosasite and smithsonite [5, 9, 38]. In many compounds three bands, one in the visible region around 600–700 nm (16,665–14,285 cm^{-1}) and two in the near-infrared at 800–900 nm and 1,100–1,200 nm (12,500–11,110 and 9,090–8,330 cm^{-1}) have been reported [28, 32, 39, 40] for Cu^{2+} ion in a distorted octahedral coordination. A report on the
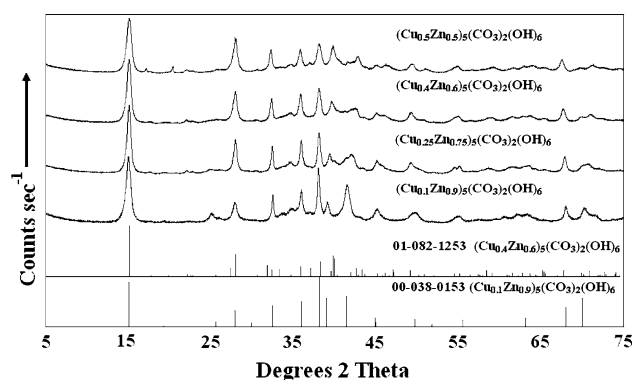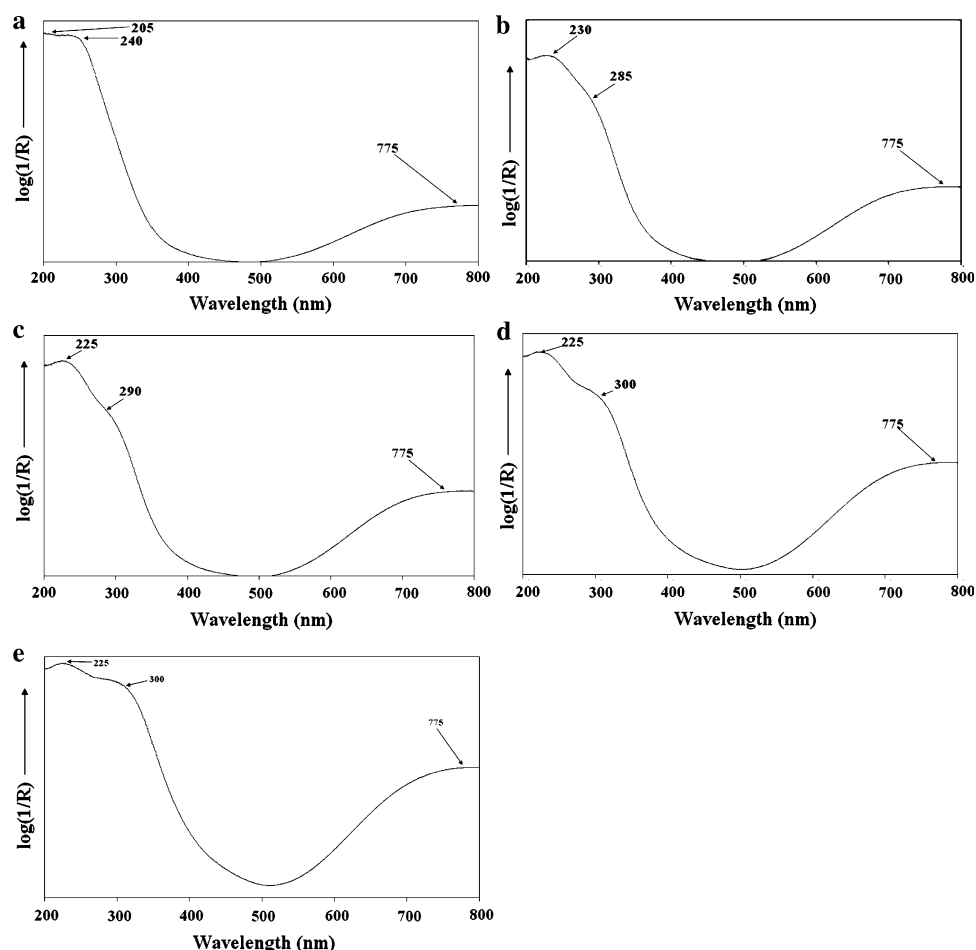

Fig. 1 X-ray diffraction patterns of synthetic aurichalcite together with standard reference materials

**Fig. 2** (**a–e**) UV–Visible spectra of synthetic aurichalcite with CZ ratios of 1:9, 1:4, 1:3. 2:3, 1:1

characterization of $Cu/ZnO/Al_2O_3$ catalysts shows one weak broad band at 800 nm (12,500 cm^{-1}) for Cu(II) ions in a distorted octahedral symmetry [41]. The spectra in the Fig. 2a–e, show a broad absorption at 775 nm (12,900 cm^{-1}) for all the five copper containing precursors from Cu:Zn ratio of 1:9, 1:4, 1:3, 2:3 to 1:1. This feature is characteristic of Cu(II) ion and is assigned to the $^2B_1 \rightarrow {}^2B_2$ transition and the first band observed in the near-infrared (Fig. 3c) around 7,600 cm^{-1} (1,315 nm) to the $^2B_1 \rightarrow {}^2A_1$ transition. Third band expected for copper ion in the visible is hidden by edge absorptions on either side of the turning points at 500 nm (20,000 cm^{-1}) in the UV–Vis spectrum. The strong band at ∼300 nm (33,330 cm^{-1}) is related to charge transfer transitions involving $Cu^{2+} - O^{2-} - Cu^{2+}$ species [42, 43]. The effect of Zn on Cu is observed in the extreme UV spectrum of Cu–ZnO catalyst for CZ ratio variation from 1:9, 1:4, 1:3, 2:3 to 1:1. The UV edge absorption derived (Fig. 2a) by CZ ratio of 1:9 resolved into a band (Fig. 2d) at 240 nm (41,665 cm^{-1}) for CZ ratio of 2:3. This band may be assigned to the charge transfer transition, $O^{2-} \rightarrow Cu^{2+}$ [42].

Near-infrared (NIR) spectroscopy

Carbonate minerals display absorption features from near-infrared to mid-infrared regions. Bands in NIR may be due to overtones of carbonate ion and hydroxyl units, in addition to the electronic transitions of the transition metal cations. The electronic bands are observed from 13,000 to 7,000 cm^{-1} (0.77–1.43 μm) and overtone bands from 7,000 to 4,000 cm^{-1} (1.43–2.50 μm). The substitution of Zn by copper in copper–zinc hydroxy carbonates provides characteristic bands with variable positions. Transition metal ion complexes, for example, carbonate minerals that include Cu(II)/Cu(II)and Fe(II) provide absorption features in the 13,000–7,000 cm^{-1} (0.77–1.43 μm) region. For carbonates several strong bands occur from 7,000 to 300 cm^{-1} (1.43–33.33 μm) due to the vibrations of the carbonate ion and OH units [36, 37].

The near-infrared spectra of synthetic aurichalcite for five compositions with varying Cu:Zn ratio, are shown in Fig. 3a–e. These spectra exhibit three distinct groups of bands. The first group consists of bands due to both

Fig. 3 (**a–e**) NIR spectra of synthetic aurichalcite with CZ ratios of 1:9, 1:4, 1:3. 2:3, 1:1
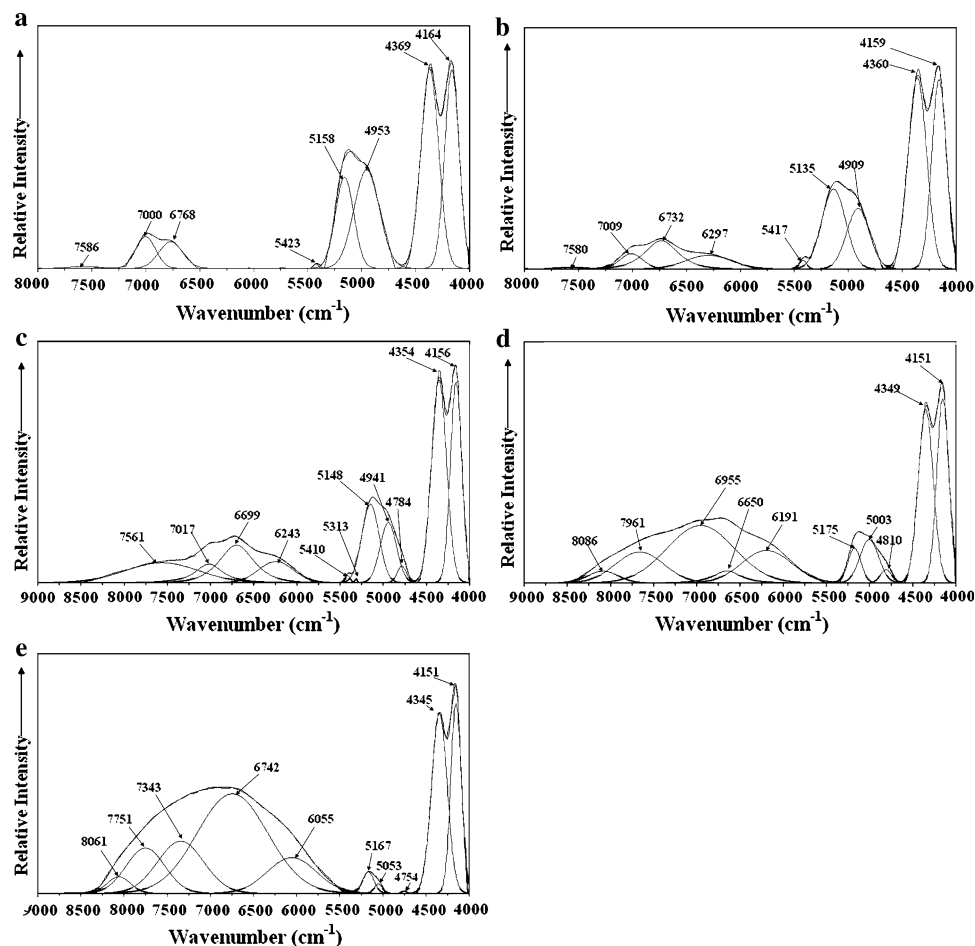
electronic and vibronic transitions in the high wavenumber region of 9,000–5,500 cm^{-1} (1.11–1.82 μm). The second and third groups from 5,500 to 4,500 cm^{-1} (1.82–2.22 μm) and 4,500 to 4,000 cm^{-1} (2.22–2.50 μm) are concerned with the overtones and combinations of vibrational modes of carbonate ion. The complexity of these band systems is resolved by the application of band component analysis, in particular, the bands in the higher energy side of the spectrum from 9,000 to 5,500 cm^{-1} (1.11–1.82 μm), where overlapping OH stretching bands and d–d transition band of Cu^{2+} occur. The spectra show a number of bands with increase in intensity from 9,000 to 4,000 cm^{-1} (1.11–2.50 μm). Four bands are well resolved in the first group around 7,600, 7,000, 6,700 and 6,200 cm^{-1} (1.32, 1.43, 1.49 and 1.61 μm). The first band is the d–d transition of Cu(II) and the latter, three bands are the overtones of the OH-stretching vibrational modes observed in the infrared from 3,400 to 3,200 cm^{-1} (Fig. 4). The report of the Raman spectrum of aurichalcite by Bouchard and Smith [44] shows a broad band for OH at 3,331 cm^{-1}. The effect of Zn on Cu is shown in the spectra (Fig. 3a, b), where Cu(II) band appeared at 7,586

and 7,580 cm^{-1} (1,318 and 1,319 nm) with weak in intensity for Cu:Zn ratio of 1:9 and 1:4. As concentration of Cu increases, the Cu^{2+} band becomes strong (Fig. 3c–e). The substitution of Cu(II) for Zn(II) in zinc–copper hydroxyl carbonates produces characteristic features with variable band positions and intensities because of the ratio of Cu to Zn may not be same in all the samples. For example, minerals of aurichalcite show variable band positions due compositional variations [5]. The carbonate stretching region of synthesized aurichalcite shows five bands around 5,200, 5,000, 4,800, 4,400 and 4,200 cm^{-1} (1.92, 2.00, 2.08, 2.27 and 2.38 μm). The assignments of bands are made to the overtones and combination modes of carbonate groups and compared with the calculated values from the fundamental modes observed in IR. The assignments of the bands for a selected set of three Cu:Zn ratios (1:3, 2:3 and 1:1) are tabulated and compared with three natural minerals of aurichalcite whose composition is similar. The shift of both Cu(II) and carbonate bands to lower wavenumbers when compared to natural minerals might be the effect of other cation impurities like Ca, Mg in the minerals. The weak band located near 5,400 cm^{-1}
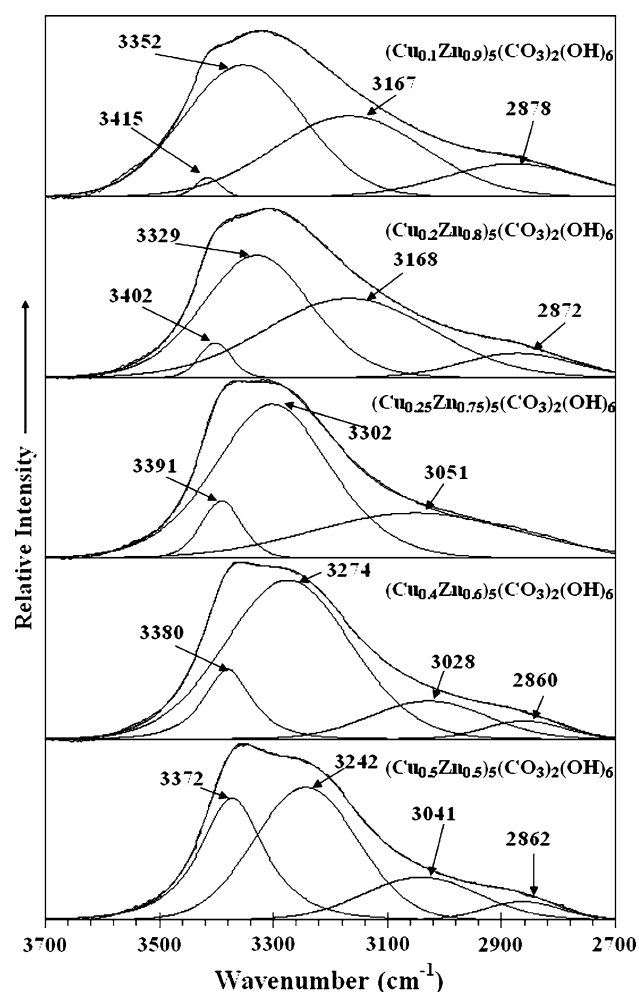
Fig. 4 Infrared spectra in the region of 2,700–3,700 cm^{-1} synthetic aurichalcite with CZ ratios of 1:9, 1:4, 1:3. 2:3, 1:1

Fig. 5 Infrared spectra in the 1,150–1,650 cm^{-1} region of synthetic aurichalcite with CZ ratios of 1:9, 1:4, 1:3. 2:3, 1:1

(1.85 μm) may be attributed to traces of adsorbed water in synthetic aurichalcite.

Mid-IR spectroscopy

The infrared spectra of OH-stretching region of the five synthetic samples of aurichalcite are shown in Fig. 4 while the spectra of carbonate stretching region is shown in two parts (Figs. 5 and 6) from 1,650 to 1,150 and 1,150 to 650 cm^{-1}. There are two main bands in the spectra of OH-stretching region from 3,400 to 3,200 cm^{-1}. The compositional variation of CZ shows variation in band position and intensity in each spectrum and the two bands are attributed to the OH-stretching vibrations. The weak band at 2,860–2,880 cm^{-1} shows traces of adsorbed water in synthetic samples. A single band 3,338 cm^{-1} was observed for aurichalcite mineral from Durango. This might be compared with 3,348 cm^{-1} for Arizona aurichalcite and

3,355 cm^{-1} for the Chihuahua mineral [16]. Band positions appearing differently in the hydroxyl stretching region of natural and synthetic aurichalcites are related to the variation of the hydrogen bond distances between the OH-units and the oxygens of adjacent carbonate units [45] (Table 1).

A broad band profile shown in carbonate stretching region from 1,650 to 1,150 cm^{-1} is attributed to the v_3 $(CO_3)^{2-}$ antisymmetric stretching modes. For CZ ratio of 1:9, two broad bands are observed at ∼1,500 and 1,400 cm^{-1} and appear as four component bands at 1,518, 1,483, 1,398 and 1,349 cm^{-1} (Fig. 5). For increase of Cu concentration, four individual bands are resolved at 1,565, 1,508, 1,408 and 1,357 cm^{-1} for Cu:Zn ratio = 1/3. The bands become sharp for Cu:Zn ratio = 2/3 and 1/1. The band positions and intensity of the v_3 vibrational modes of carbonate ion depends on the ratio of CZ. Spectra in the second part of the carbonate stretching region 1,150–650 cm^{-1} are depicted in Fig. 6. The low wavenumber of the carbonate stretching
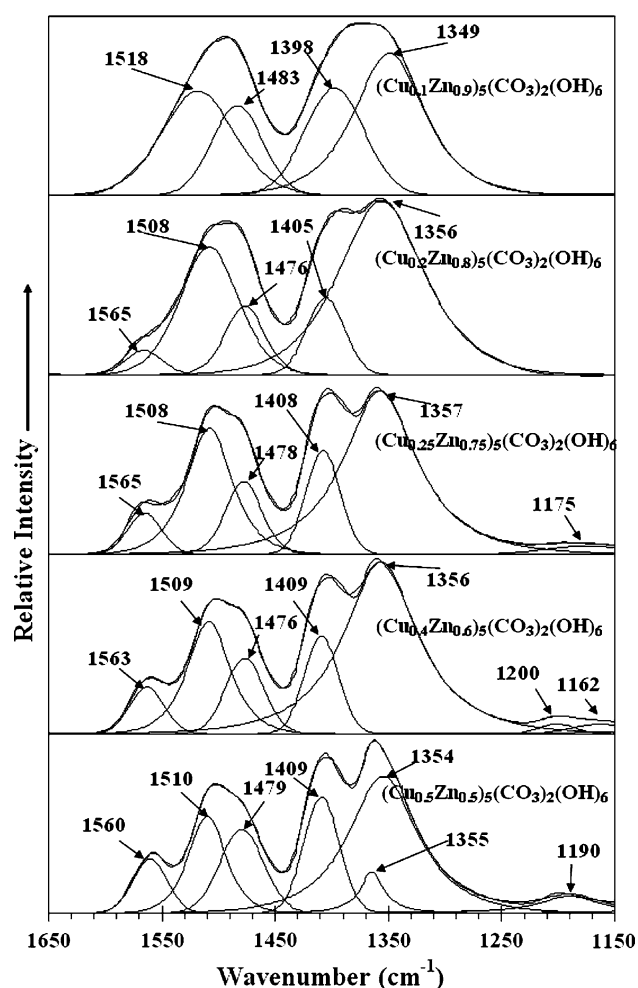
Fig. 6 Infrared spectra in the 650–1,150 cm⁻¹ region of synthetic aurichalcite with CZ ratios of 1:9, 1:4, 1:3. 2:3, 1:1

region is a complex profile and is resolved into a number of bands. The v_2 bending modes for carbonates vary between 824 and 833 cm⁻¹. On either side of this sharp band, two other modes at $\sim 1{,}050$ and 740 cm⁻¹ are v_1 symmetric stretching vibration and v_4 bending modes $(CO_3)^{2-}$ ion. The observation of multiple bands in symmetric stretching and bending regions confirms the reduction of symmetry from D_{3h} to C_{2v}/C_s for $(CO_3)^{2-}$ ion in aurichalcite. Raman spectroscopic study of aurichalcite reported by Frost et al. [16] shows the ranges of vibrational modes for carbonate ion are $(v_1 = 1{,}072–1{,}060$ cm⁻¹, $v_2 = 850–800$ cm⁻¹, $v_3 = 1{,}500–1{,}300$ cm⁻¹ and $v_4 = 750–720$ cm⁻¹. The analysis of IR data is in harmony with the reported Raman spectra of aurichalcite minerals.

Conclusions

The catalyst activity of copper–zinc oxides is known to depend on the catalyst precursor. For example, such

Table 1 Assignments of UV–Visible and NIR bands of synthetic and natural aurichalcite minerals

Synthetic aurichalcite samples						Natural aurichalcite minerals[a]						Calculated		Suggested assignment	Reported[b]	
Cu:Zn = 1:3		Cu:Zn = 2:3		Cu:Zn = 1:1		Aurichalcite1 (Durango, Mexico)		Aurichalcite2 (Chihuahua, Mexico)		Aurichalcite3 c(Arizona, USA)						
λ (nm)	ν (cm⁻¹)	λ (nm)	ν (cm⁻¹)	λ (nm)	ν (cm⁻¹)	λ (nm)	ν (cm⁻¹)	λ (nm)	ν (cm⁻¹)	λ (nm)	ν (cm⁻¹)	λ (nm)	ν (cm⁻¹)		λ (nm)	ν (cm⁻¹)
775	12900	775	12900	775	12900	860	11650p	845	11865p	870	11465			$^2B_1 \to {}^2B_2{}^t$	~800	~12500
1325	7561	1235		1240		915	10940	890	11230	925	10820p			$2B_1 \to A_1{}^t$		
		1255	8086p	1290	8061p										~1400	~7140
			7961		7751											
1425	7017	1440	6955	1360	7343	1490	6705	1400	7145	1420	7040	1470–1565	6800–6400	$2v_3{}^c$		
1495	6699	1505	6650	1485	6742	1565	6400	1520	6585	1450	6890			$v_3{}^c$		
1600	6243	1615	6191	1650	6055	1620	6165	1630	6140	1615	6190			$v_3{}^c$		
1850	5410					1850	5400	1850	5405	1835	5455	1595–1645	6260–6080	$(v_2 + v_3)^c$	~1900	~5260
1945	5148	1930	5175	1935	5167	1950	5135	1955	5120	1915	5220	1955	5110	$(2v_1 + 2v_3)^d$	1850–1870	5405–5348
2025	4941	2000	5003	1980	5053	2000	5010	2000	5000	1970	5075	2085	4795	$(3v_1 + 2v_2)^d$	1970–2000	5076–5000
2090	4784	2080	4810	2105	4754	2230	4480	2210	4525s	2215	4510	2222	4500	$(2v_3 + 2v_4)^d$	2120–2160	4717–4630
								2250	4440							

Table 1 continued

Synthetic aurichalcite samples						Natural aurichalcite minerals[a]						Calculated		Suggested assignment	Reported[b]	
Cu:Zn = 1:3		Cu:Zn = 2:3		Cu:Zn = 1:1		Aurichalcite1 (Durango, Mexico)		Aurichalcite2 (Chihuahua, Mexico)		Aurichalcite3 c(Arizona, USA)						
λ (nm)	ν (cm⁻¹)	λ (nm)	ν (cm⁻¹)	λ (nm)	ν (cm⁻¹)	λ (nm)	ν (cm⁻¹)	λ (nm)	ν (cm⁻¹)	λ (nm)	ν (cm⁻¹)	λ (nm)	ν (cm⁻¹)		λ (nm)	ν (cm⁻¹)
2295	4354	2300	4349	2300	4345	2275	4395	2300	4350	2300	4355	2390	4185	$(\nu_1 + 2\nu_2 + 2\nu_4)$[d]	2300–2350	4348–4255
2405	4156	2410	4151	2410	4151	2395	4175	2405	4160	2385	4195		4065	$(\nu_1 + 2\nu_3)$[d]	2500–2550	4000–3922

[t] Electronic transition of Cu^{2+} ions

[a] Reported data on NIR spectroscopy of aurichalcites minerals [5]

[b] Range of band positions reported by Hunt and Salisbury [37]

[c] Overtones and combination modes calculated from OH vibrational modes of ν_3 and ν_2 observed in the IR spectra of synthetic aurichalcite at 3,400–3,200 and 2,860–2,880 cm⁻¹

[d] Overtones and combination modes of $(CO_3)^{2-}$ fundamentals calculated from the observed data in the IR spectra of synthetic aurichalcite

($\nu_1 = 1{,}045$, $\nu_2 = 830$, $\nu_3 = 1{,}510$ and $\nu_4 = 740$ cm⁻¹)

Abbreviations: p-component; s-shoulder

copper–zinc oxides can be used as photocatalysts for the wet photocatalytic oxidation of recalcitrant organics in potentially potable water and aqueous media. These oxide mixtures also have biological activity and may be used for the removal of biological organisms from potentially potable water. The use of aurichalcite in synthesising these catalysts precursors rests with the thermal decomposition of the aurichalcite to prepare mixed oxides which are mixed at the atomic level rather than the particle scale.

Aurichalcite was synthesized by varying Cu:Zn ratio between the range 1:9 and 2:3. Characterization of aurichalcite shows two broad bands in the electronic spectrum at ~7,600 and 12,900 cm⁻¹ (1,315 and 775 nm) for Cu^{2+} ion in a distorted octahedral symmetry. The effect of increasing the Cu:Zn ratio results in increased intensity and band position in the electronic spectrum due to increasing molar ratio of Cu^{2+}.

The shifts of Cu(II) and carbonate bands to lower wavenumbers of synthetic minerals, when compared with natural minerals might be the result of other cation impurities like Fe^{2+}, Ca, Mg in the natural minerals which negate these shifts. A weak band near 5,400 cm⁻¹ (1.85 μm) indicates traces of adsorbed water in synthetic aurichalcite. The band positions and intensity of the ν_3 vibrational modes of carbonate ion depends on the ratio of CZ. The bands become sharp for Cu:Zn ratio = 2/3 and 1/1. Compositional variations are controlled by Cu:Zn ratio. The analysis of IR data agrees closely with the reported Raman spectra of aurichalcite minerals. The spectra of synthetic aurichalcite may be used as a basis to analyse the spectra of natural hydroxy-carbonates in particular, Cu–Zn carbonates.

References

1. Braithwaite RS, Ryback G (1963) Mineral Mag 33:441
2. Jambor JL (1964) Can Mineral 8:92
3. Jambor JL, Pouliot G (1965) Can Mineral 8:385
4. Herman RG, Bogdan CE, Kumler PL, Nuszkowski DM (1993) Mater Chem Phys 35:233
5. Reddy BJ, Frost RL (2007) J Near Infrared Spectrosc 15:115
6. Frost RL (2006) J Raman Spectrosc 37:910

7. Frost RL, Wain DL, Martens WN, Reddy BJ (2007) Polyhedron 26:275
8. Frost RL, Wain DL, Martens WN, Reddy BJ (2007) Spectrochim Acta Part A 66:1068
9. Frost RL, Reddy BJ, Wain DL, Martens WN (2007) Spectrochim Acta Part A 66:1075
10. Ghose S (1964) Acta Cryst 17:1051
11. Williams PA (1990) Oxide zone geochemistry. Ellis Horwood Ltd, Chichester
12. Harding MM, Kariuki BM, Cernik R, Cressey G (1994) Acta Cryst B50:673
13. Sengupta G, Sharma RK, Sharma VB, Mishra KK, Kundu ML, Sanyal RM, Dutta S (1995) J Solid State Chem 115:204
14. Pollard AM, Spencer MS, Thomas RG, Williams PA, Holt J, Jennings JR (1992) J Appl Catal A85:1
15. Porta P, De Rossi S, Ferraris G, Pompa F (1991) Solid State Ionics 45:35
16. Frost RL, Hales MC, Reddy BJ (2007) Polyhedron 26:3291
17. Herman RG, Klier K, Simmons GW, Finn BP, Bulko JB, Kobylinski TP (1979) J Catal 56:407
18. Himelfarb PB, Simmons GW, Klier K, Herman RG (1985) J Catal 93:442
19. Stacey MH, Shannon MD (1985) In: Barret P, Dufour L (eds) Reactivity of solids. Elsevier, Amsterdam, p 713
20. Clausen BS, Steffensen G, Fabius B, Villadsen J, Feidenhans'l R, Topsøe H (1991) J Catal 132:524
21. Fujita S, Satriyo AM, Shen GC, Takezawa N (1995) J Catal Lett 34:85
22. Fujita S, Usui M, Ito H, Takezawa N (1991) J Catal 157:403
23. Petrini G, Garbassi F (1991) J Catal 90:113
24. Hoppener RM, Doesburg EBM, Scholten JJF (1986) Appl Catal 25:109
25. Hadden RA, Lambert PJ, Ranson C (1995) Appl Catal A122:L1
26. Stone FS, Waller D (2003) Top Catal 22:305
27. Billing DE, Hathaway BJ (1968) J Chem Soc A:1516
28. Hathaway BJ, Billing DE (1970) Coord Chem Rev 5:143
29. Sarma KBN, Reddy BJ, Lakshman SVJ (1982) Phys Lett 92A:305
30. Reddy KM, Jacob AS, Reddy BJ, Reddy YP (1987) Phys Stat Sol (b) 139:K14
31. Reddy BJ, Frost RL, Martens WN (2005) Mineral Mag 69:155
32. Lever ABP (1984) Inorganic electronic spectroscopy. Elsevier, Amsterdam, p 19
33. Fujita S, Kanamori Y, Satriyo AM, Takezawa N (1998) Catal Today 45:241
34. Millar GJ, Holm IH, Uwins PJR, Drennan J (1998) J Chem Soc, Faraday Trans 94:593
35. Frost RL, Weier ML, Erickson KL (2004) J Therm Anal Calorim 76:1025
36. Adams JB (1974) J Geophys Res 79:4829
37. Hunt GR, Salisbury JW (1971) Mod Geol 2:23
38. Frost RL, Reddy JB, Wain DL, Hales MC (2006) J Near Infrared Spectrosc 14:317
39. Ballhausen CJ (1962) Introduction to ligand field theory. McGraw-Hill, New York
40. Reddy KM, Jacob AS, Reddy BJ, Reddy YP (1987) Phys Stat Sol (b) 139:K145
41. Turco M, Bagnasco G, Costantino U, Marmottini F, Montanari T, Ramis G, Busca G (2004) J Catal 228:43
42. Velu S, Suzuki K, Okazaki M, Kapoor MP, Osaki T, Ohashi F (2004) J Catal 194:373
43. de Carvalho MCNA, Passos FB, Schmal M (2000) Appl Catal A193:265
44. Bouchard M, Smith DC (2007) Spectrochim Acta Part A 59:2247
45. Libowitzky E (1999) Monatsh Chem 130:1047